Journal of The Electrochemical Society, **161** (9) F906-F917 (2014)
0013-4651/2014/161(9)/F906/12/$31.00 © The Electrochemical Society

The Mechanism of Oxygen Reactions at Porous Oxide Electrodes
III. Water Oxidation Catalysis at RuO_2/NiO Mixed Oxide Electrodes

Ian J. Godwin,*,z Richard L. Doyle, and Michael E. G. Lyons

School of Chemistry and AMBER, CRANN Research Institute, Trinity College Dublin, College Green, Dublin 2, Ireland

RuO_2/NiO mixed oxide electrodes prepared by thermal decomposition were examined as potential water oxidation catalysts. Addition of just 10 mol% RuO_2 to a NiO electrode was found to decrease the oxygen evolution reaction (OER) onset potential by 20% with increasing additions having significantly diminishing returns. The OER current densities for the RuO_2/NiO electrode were found to increase when preconditioned by application of prolonged polarization regimes with the Tafel slope also decreasing when conditioned. NiO prepared by thermal decomposition was found to behave in a similar manner to other nickel oxides prepared using different methodologies and we propose a similar OER mechanism based on the kinetic data obtained using the surfaquo group concept. A dual barrier model was used to rationalize the fractional reaction order of ca. 0.5 observed for RuO_2.

Manuscript submitted March 3, 2014; revised manuscript received June 5, 2014. Published June 12, 2014.

Alkaline water electrolysis has become an area of intense international research due to the need for a method to efficiently produce large amounts of molecular hydrogen which would be required for a potential hydrogen economy. Currently one of the main drawbacks limiting the widespread use of this technology is in the large anodic overpotential associated with the oxygen evolution reaction (OER). Dimensionally Stable Anodes (DSA) are one such technology which can effectively catalyze the OER thus increasing the overall efficiency of the water electrolysis reaction. DSA electrodes consist of an underlying electrochemically inert valve metal substrate such as titanium or tantalum, coated usually with an oxide or mixed oxides of platinum group metals (PGM). To date, they have been employed in many industrial processes such as the chlorine evolution reaction,[1] electrowinning of metal ores[2] and as an anode for use in industrial water electrolyzers.[3] Herein, we focus attention on the latter use in an alkaline environment. DSA electrodes based on IrO_2/RuO_2 currently exhibit one of the lowest overpotential for the oxygen evolution reaction (OER), which is said to be the 'bottleneck' or rate determining step in a water electrolyzer cell at standard operating currents. PGM oxide mixtures such as IrO_2/RuO_2 as studied by Lyons,[3,4] Trasatti[4–6] and others on Ti exhibit extremely low OER overpotentials (ca. 0.20–0.25 V) and display long term stability in strong alkaline conditions required for an alkaline water electrolyzer setup. However, the main drawback in fully utilizing PGM oxide based DSA electrodes is in the high cost associated with these metals, and thus, significant international research is being currently focused on finding cheaper alternatives which still display relatively low overpotentials. This paper focuses on minimizing the amount of expensive PGM oxides, RuO_2 in this case which currently costs $2.1 million/ton, required by combining them with low cost NiO, currently $14 000/ton, which displays relatively low overpotentials for the OER[7–9] but at a significantly lower cost. A range of RuO_2/NiO compositions was studied herein and the effect of varying the relative mole percent of each oxide on the redox properties, reaction order and OER kinetics and mechanism will be studied using the traditional electrochemical tools of cyclic voltammetry and steady state Tafel plots.

Experimental

All experiments were conducted in a conventional three electrode cell kept at 25°C connected to a Gamry 600 model potentiostat. All metals and metal salts used were supplied by Alfa Aesar and are > 99.99% metals basis. A graphite rod was used as the counter electrode and Hg/HgO (CH instruments) was employed as the reference electrode. The iR drop was calculated using high frequency potentiostatic impedance spectroscopy and all electrochemical data reported has been corrected accordingly. All electrochemical measurements were carried out in 1 M NaOH unless otherwise indicated. The RuO_2/NiO mixed oxide films were made up by making separate 0.2 M solutions of $RuCl_3.xH_2O$ and $Ni(NO_3).6H_2O$ in butanol. These solutions were then mixed in the desired ratios and the resulting solution was painted onto the exposed Ti wire electrode with a typical geometric area of 1 cm^2. The electrodes were dried at 80°C for 5 min to evaporate off excess solvent and further annealed at 425°C for 10 minutes to convert the metal salt to the metal oxide. This process was repeated several times until a sufficiently thick loading was obtained. The electrode was finally annealed at 425°C for 3 hours to ensure complete conversion to the oxide. Scanning electron microscopy was carried out using a Carl Zeiss Ultra SEM with an accelerating electron voltage of 5 kV. Energy dispersive X-ray analysis was obtained using Oxford Instruments X-Max EDX detector. EDX confirmed the composition of the mixed oxide films and was carried out at 15 kV unless otherwise indicated. The mixing preparation method was found to be accurate to within 2 mol% of the predicted composition. Although the three hour annealing time chosen was sufficient to decompose the precursor chloride salt some small residual chloride (ca. 1%) remained combined with negligible nitrate present. All references to the relative mole fractions will be described as additions of RuO_2 to a NiO electrode i.e. a 25 mol% RuO_2 electrode describes a 75% NiO electrode and so on. All mixed oxide compositions stated refer to the metal mole percentage. Powder X-ray diffraction (PXRD) was carried out using a Bruker Duo with a Cu kα source ($\lambda = 1.54$ Å) on all mole fractions to determine the oxide phase composition. In all cases the Tafel slope was calculated in the linear potential region immediately after OER onset. The voltammetric charge q or q* for use in the normalization of the Tafel plots and for calculation of the turnover frequency[10] was calculated by integrating the area under the oxidation sweep of the relevant voltammogram at 40 mV/s in 1 M NaOH between hydrogen evolution and oxygen evolution.

Results and Discussion

Physical characterization.— PXRD confirmed that we have ruthenium oxide and nickel oxide in the form of RuO_2 and NiO respectively which is in good agreement with others given the experimental conditions chosen.[11,12] As shown in Fig. 1a-1d RuO_2 and indeed all oxide films containing RuO_2 prepared by thermal decomposition display the characteristic mud-cracked appearance associated with RuO_2 films prepared previously by others.[4] The film interspacings and thickness are typically on the order of a micron in magnitude, verified using SEM, with thickness and spacing being highly dependent on number of applied coatings and length of annealing time/temperature respectively. Nickel oxide formed by thermal decomposition in comparison, displays a layered type structure with individual lamellae overlapping each other as seen in Fig. 1e. Rather interestingly, all oxide mixtures studied display surface nanoparticles of between 10–200 nm in diameter distributed across all faces of the oxide film. To best of our

*Electrochemical Society Student Member.
zE-mail: godwini@tcd.ie

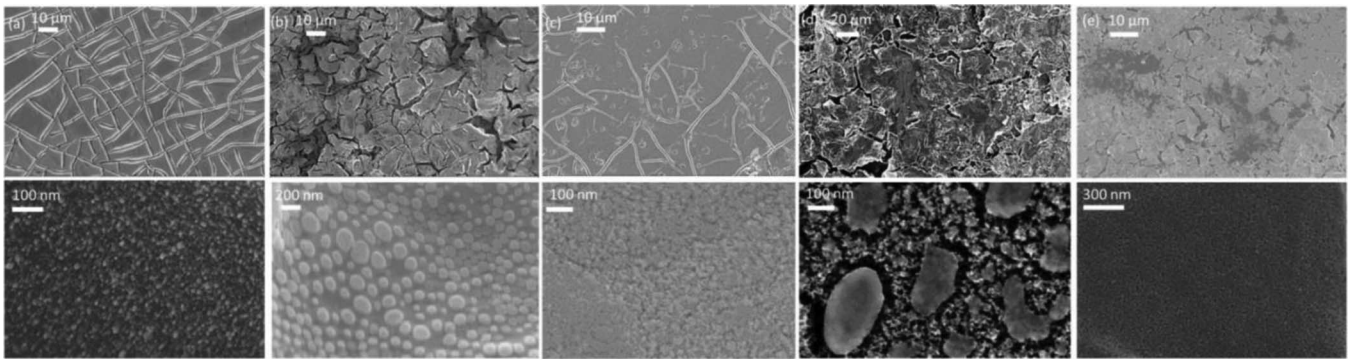

Figure 1. SEM image of the as prepared (a) RuO_2 film prepared by thermal decomposition (b) 10% Ni 90% Ru (c) 50% Ni 50% Ru (d) 90% Ni 10% Ru (e) NiO. The corresponding images underneath are simply higher resolution images of the above.

knowledge this is the first time such nanoparticles have been observed on RuO_2 and NiO films synthesized in this fashion. We do not believe however that our discrete oxide films are in fact any different to those reported earlier by people such as Trasatti[5] and Srinivasan.[13] It is most probable that this observation is just due to higher resolution imaging being performed in the present work. The size of these surface nanoparticles for the discrete oxides were found to be on the order of 10 nm in diameter and are uniformly coated on the oxide surface. Assuming a cubic shape, this would give a surface area of 500 nm^2 for the individual nanoparticles which compares to an area of 0.34 nm^3 calculated for a surface active (surfaquo) group by Lyons and Burke in part I of this series.[3] Therefore one would expect that there are > 1000 of these surfaquo groups on each nanoparticle site. We hence propose that these catalytically active surface nanoparticles, in part at least, account for the excellent OER activity displayed by both oxides owing to their large available surface area.

Indeed as stated previously, all mixed oxides as shown in Fig. 1 were shown to display varying morphology on the nanoscale indicating a strong dependence on the relative mole% of each oxide in the mixture. However, we could see no trend in size/shape of these nanoparticles with varying the relative mole fraction but it does indicate the strong dependence on the oxide mixture on the nanoscale morphology of each oxide. Oxide mixtures containing $\leq$50% Ru were found to have multifaceted microparticles, typically with a diameter of several microns, evenly dispersed across the surface. EDX analysis confirms that these particles are solely composed of RuO_2. This observation leads us to believe that the mixed oxide electrodes in this composition range undergo surface enrichment by RuO_2 and hence surface properties are, to a large extent, dominated by RuO_2 and not NiO. This assumption will be further supported later in the next section using electrochemical techniques. EDX analysis indicates that Ni:Ru is approximately present in the bulk in a ratio of 3:1 This surface enrichment by RuO_2 has been suggested for Co-Ru mixed oxide electrodes made by Da Silva and co-workers[14] and Trasatti and Krstajic,[15] based only on electrochemical data. This experimental observation of surface enrichment is also in accordance with DFT studies carried out by Novell-Leruth and co-workers[16] who suggest that due to the low surface energy associated with RuO_2, it would preferentially be found on the surface in many mixed oxide systems.

Electrochemical characterization.— The effect of varying the relative mole fraction of RuO_2 in the mixed oxide system on the voltammetric response can be seen in Fig. 2. The two prominent redox couples that are observed in the oxides studied are Ni(II/III), Fig. 2a, and Ru(VI/VII), Fig. 2f, redox couples which occur at 0.51 V and 0.45 V for the oxidation peaks and 0.40 V and 0.44 V for the reduction peaks respectively. The redox behavior of surface immobilized oxyruthenium groups is assumed to involve the simultaneous loss or gain of protons and electrons and be represented by the following equations:[4]

$$\text{Ru(III/IV)} \quad (-O-)_2RuOH(OH_2)_3 + OH^- \rightarrow (-O-)_2Ru(OH)_2(OH_2)_2 + H_2O + e^- \quad [1]$$

$$\text{Ru(IV/VI)}: \quad (-O-)_2Ru(OH)_2(OH_2)_2 + 2OH^- \rightarrow (-O-)_2Ru(OH)_4 + 2H_2O + 2e^- \quad [2]$$

$$\text{Ru(VI/VII)}: \quad (-O-)_2Ru(OH)_4 + OH^- \rightarrow (-O-)_2RuO(OH)_3 + H_2O + e^- \quad [3]$$

In aqueous alkaline environment NiO will undergo the following reaction:

$$NiO + H_2O \rightarrow Ni(OH)_2 \quad [4]$$

For the NiO (and analogously for RuO_2) film prepared by thermal decomposition, we assume that it consists of a thick compact oxide layer with a thinner hydrated outer layer which is formed when subjected to potential multicycling in basic media. This hydrated form of nickel oxide is envisaged as an amorphous microdispersed layer where nickel atoms are joined by bridging oxygens. This 'duplex layer' model was first proposed by Burke and O'Sullivan[17] for hydrous rhodium oxide electrodes prepared from potential multicycling a polycrystalline rhodium electrode in aqueous media. We attempt to liken our thermal nickel oxide electrodes to the hydrous nickel oxide electrodes we have prepared previously.[9] One can justify this assumption from the observed hydration effect, discussed in the next section, observed for the thermal NiO electrode upon potential multicycling which is akin to the observed effect seen for a hydrous nickel electrode when subjected to the same cycling. Another common factor between the two types of nickel electrodes, is that the Ni(II/III) transition for both, is suggested to be the same, and can be described by the simplified equation:[9]

$$Ni(OH)_2 + OH^- \rightarrow NiOOH + H_2O + e^- \quad [5]$$

If we assume that both types of nickel oxide have a similar hydrated outer layer, both electrodes are proposed to consist of the same catalytic NiOOH before oxygen evolution though further spectroscopic studies are required to validate this. NiOOH is said to be 'the right type of oxide'[18] for the OER and its catalytic properties partly come from its excellent electrical conductivity as compared with $Ni(OH)_2$.[19] One argument which could be used to discard the assumption that the thermal NiO film is similar to the hydrous nickel oxide film would rest on the fact that the observed redox peak potentials and OER onset potential for the two materials vary from each other by up to 50 mV. This could suggest a different redox chemistry operating, with the relevant potentials observed for thermal NiO electrode usually being more positive than the multicycled polycrystalline nickel oxide film. We however suggest that this difference in observed peak

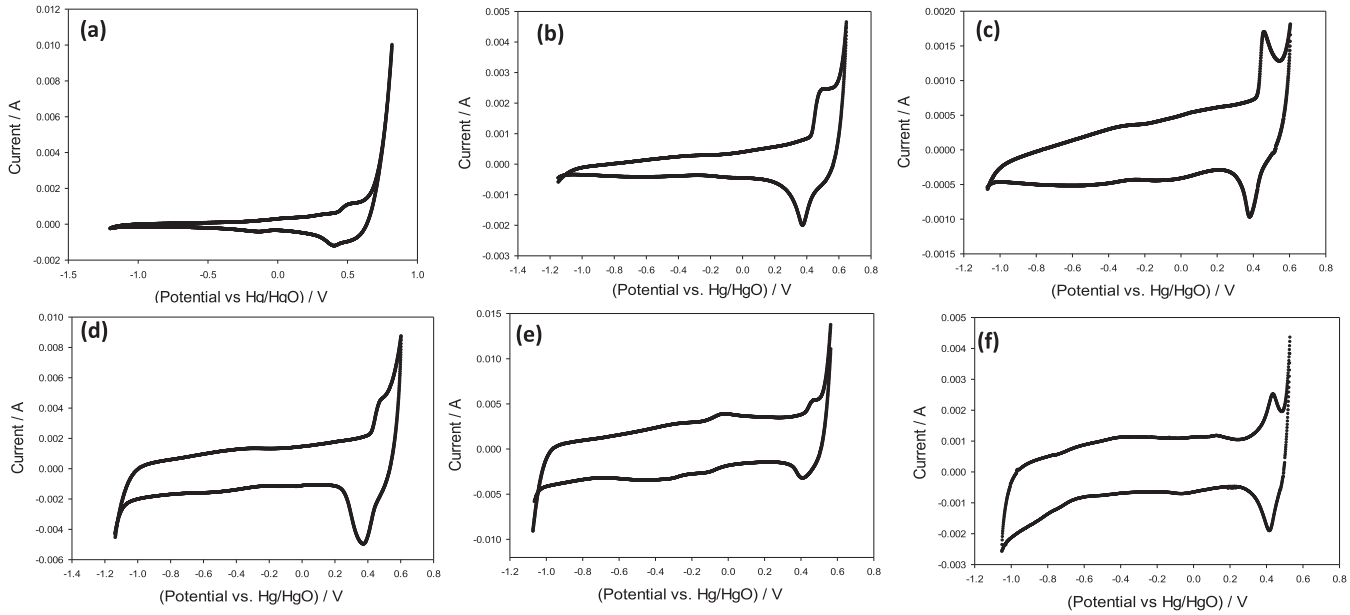

Figure 2. Typical voltammetric response of (a)100 mol% NiO (b) 10 (c) 25 (d) 50 (e) 90 (f) 100 mol% RuO_2 on a Ti substrate. Electrolyte is 1 M NaOH. Scan rate: 40 mV s^{-1}. Potentials quoted against Hg/HgO.

potentials can be attributed to the underlying bulk conductivity being lower for the thermal NiO compared with that of the polycrystalline nickel oxide electrode, the latter film would be expected to be thin. This lower conductivity would account for the observed increase in redox potentials and oxygen evolution onset potential for the thermal NiO electrode. We can support this statement by looking at Fig. 3 which shows the high frequency impedance response for a hydrous nickel oxide electrode and the NiO electrode prepared herein. At high frequencies we can expect to only see impedance contributions from the solution resistance and the intrinsic oxide film resistance. Since we are using a fixed cell geometry and electrolyte for each oxide film we can assume the solution resistance is constant and therefore the apparent film resistance (using this this preparation procedure) for both oxides is approximately the same. Even at very high frequencies >100 000 Hz the resistance is ca. 25% lower for the hydrous nickel oxide film. Thus we propose this increase in film resistance to account for the broader and more positive peak potentials observed for NiO over the hydrous nickel oxide films we have prepared previously.

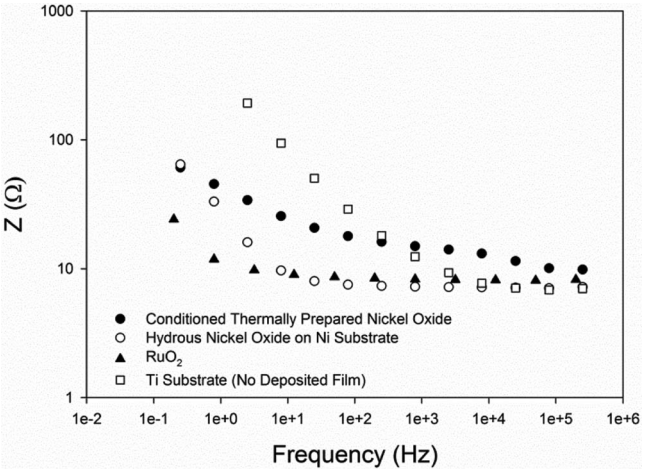

Figure 3. Comparison of the high frequency potentiostatic electrochemical impedance response of oxide films.

Now, utilizing the previous assumption of the similarities between the two nickel oxides, the main charge storage peak for NiO i.e. the Ni (II/III) redox couple, can be more accurately described by the following equation which has been rationalized previously for the hydrous nickel oxide electrode:[20]

$$[Ni_2(OH)_6(OH_2)_3]_n^{2-} + 3nOH^- \rightarrow [Ni_2O_3(OH)_3(OH_2)_3]_n^{3-} + 3nH_2O + 2ne^- \quad [6]$$

Relatively small additions of RuO_2 to NiO film changed the observed voltammetric response significantly. With addition of just 10 mol% RuO_2, as given in Fig. 2b, the oxidation peak at ca. 0.5 V is noticeably sharper than that of the pure NiO film with the peak potential remaining relatively invariant. The same can be seen for the corresponding reduction peak at 0.4 V but in this case, it experiences a negative peak potential shift of ca. 0.035 V indicating that the oxidized Ni(III) state becomes more stable with increasing additions of RuO_2. The electrochemical reversibility of the system was also found to significantly increase with increasing additions of RuO_2. Delta E_p for the main redox peaks was found to vary from ca. 100 mV for NiO to ca. 20 mV for an RuO_2 electrode.

Potential Multicycling and Activation of Mixed Oxide films for the OER.—As discussed previously, the charge capacity associated with the Ni(II/III) surface redox transition increases significantly upon successive potential multicycling (Fig. 4a). Similar effects have been reported by this group and others when oxidized Ni,[21] Fe,[22] Co,[23] Rh[24] and Ir[25] are subjected to repetitive potential multicycling regimes in basic aqueous media. This effect has been shown to be due to the disruption of the bulk parent metal atoms upon oxidation with coordination of aqueous species upon subsequent reduction thus forming an amorphous hydrated layer on top of the more compact surface oxide with the film getting thicker with each subsequent cycle at the expense of the parent bulk material. A significantly more comprehensive description of this growth mechanism is given in a review by Lyons and Burke.[26] We propose a similar growth mechanism to account for the growth observed with thermally prepared nickel oxide upon successive potential multicycling. The Ni(II/III) redox couple shows one oxidation peak and two reduction peaks during cycling. The oxidation peak at ca. 0.58 V and the extremely broad reduction peak at 0.05 V can be attributed to the oxidation and reduction of the hydrous layer respectively due to these peaks increasing in charge

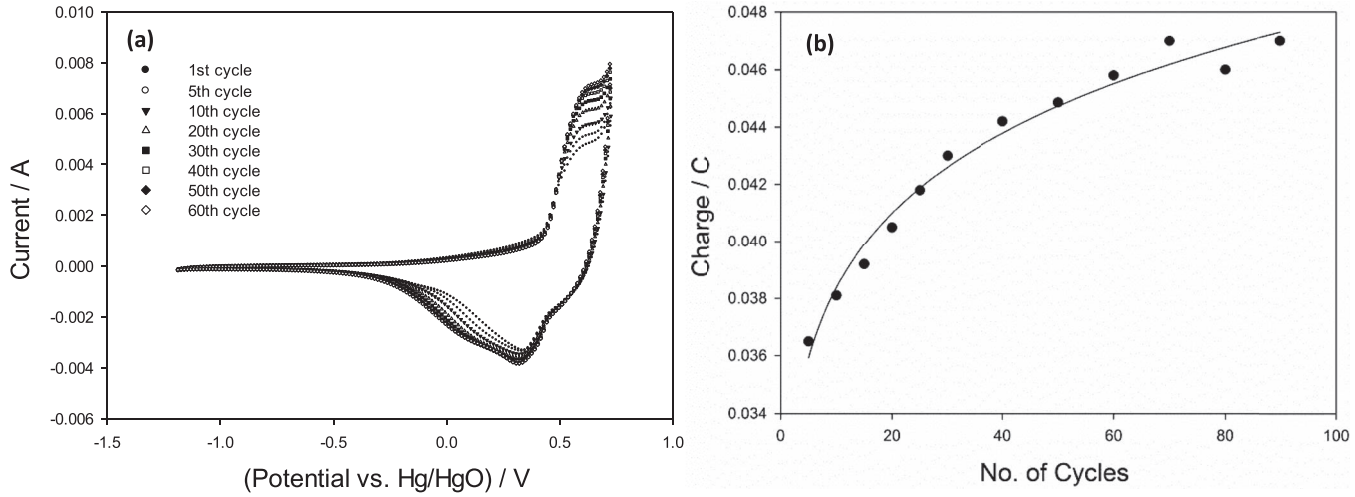

Figure 4. Cyclic voltammogram of a potential multicycled NiO electrode between −1.2 V and 0.75 V for 60 cycles. (b) Voltammetric charge a NiO electrode vs. number of potential multicycles. Potentials quoted against Hg/HgO.

most significantly upon cycling. The reduction peak at ca. 0.33 V therefore can be attributed to the reduction of the inner compact bulk oxide. The hydrous layer is therefore more stable than the inner compact layer due to the need of a greater reduction potential to reduce it back to the Ni(II) form. Outer hydrous oxides have been suggested to be more stable than the inner compact oxide by Lyons and Burke.[26] One oxidation peak with two corresponding reduction peaks is also observed for the hydrous nickel oxide electrode which draws more similarities between both oxide electrodes. As shown in Fig. 4b, the charge of the oxidation peak increases and levels off after ca. 60 cycles indicating little or no further hydration of the NiO film occurring on subsequent cycling. Indeed, all oxide compositions studied containing nickel were found to experience some degree of hydration. Fig. 5a shows the voltammetric response of a 50 mol% RuO_2 electrode subjected to 120 potential cycles. We again see a similar increase with charge, however, the charge was found to equilibrate after ca. 30 cycles despite the peak current increasing and the narrowing of the main oxidation charge storage peak at ca. 0.5 V upon successive cycling. This could indicate that though there is no increase in the amount of reaction sites, indicated by no further increase in charge, the reaction sites however are becoming more uniform in nature which is suggested by the sharpening and narrowing of the oxidation peak. This increase in charge upon potential multicycling was not seen for a pure RuO_2 electrode possibly due to the Ru-O bond strength being too great to break, which is necessary for such hydration to occur in the potential region examined. The Ru-O bond has strength of 528 kJ mol^{-1} while the Ni-O bond strength was shown to be 384 kJ mol^{-1}.[27]

Another observed feature for NiO and RuO_2 and all oxide compositions in-between was the activation of the film when subjected to polarization regimes in the OER potential region. The activation of the electrodes was experienced in two ways. First, the main redox couple be it Ru(VI/VII) or Ni(II/III) was found to increase in charge upon vigorous polarization. Secondly the measured Tafel slope, which indicates the relative increase in OER current density per increase in unit potential, was found to decrease until a minimum was reached which indicates an increase in catalytic activity after the electrode had been preconditioned by applying a large prolonged (300 mA cm^{-2}) current density. For an RuO_2 electrode, running three successive Tafel scans followed by application of a current density of 300 mA cm^{-2} for 30 minutes, as shown in Fig. 5b, the current density was found to increase by a factor of four at a fixed overpotential of 0.4 V with the Tafel slope in this case remaining relatively invariant with a value of 47–50 mV dec^{-1}. This increase in current density with an invariant Tafel slope upon polarization indicates a reduction in overpotential for the OER at a fixed current density suggesting the 'activated' mixed oxide is more effectively lowering the barrier for the OER. This could possibly be due to a surface roughening effect which would increase the accessible active surface area. NiO in comparison, experiences markedly less of an increase in current density upon polarization but however, unlike RuO_2, it does show a decrease in Tafel slope which has a value of ca. 78 mV dec^{-1} for a freshly prepared electrode and decreases to ca. 63 mV dec^{-1} when subjected to several Tafel scans indicating an increase in catalytic activity of the material due to conditioning and most likely arises from the formation of the catalytic, more conductive, NiOOH upon polarization as suggested previously. The Tafel slope value of 60 mV dec^{-1} for thermally prepared NiO is in good agreement with values obtained by Juodkazis and co-workers for nickel oxide prepared using a similar methodology.[28] Indeed a Tafel slope of 60 mV dec^{-1} has been obtained for hydrous nickel oxides which further supports the linkage between our thermal NiO and such oxides.[21] Trotochaud and co-workers[29] have shown when nanometre thick NiO films are

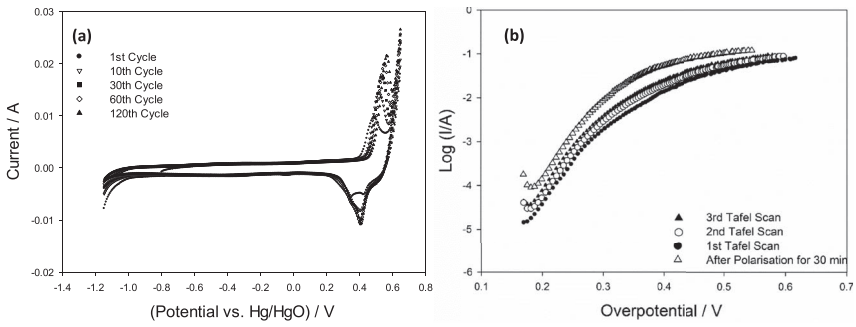

Figure 5. (a) Voltammetric response of a 50 mol% Ru electrode cycled between −1.2 V and 0.7 V for 120 cycles. Scan rate: 40 mV s^{-1}. Potentials quoted against Hg/HgO. (b) Steady state polarization curves for RuO_2. Electrolyte is 1 M NaOH. Scan rate: 1 mV s^{-1}.

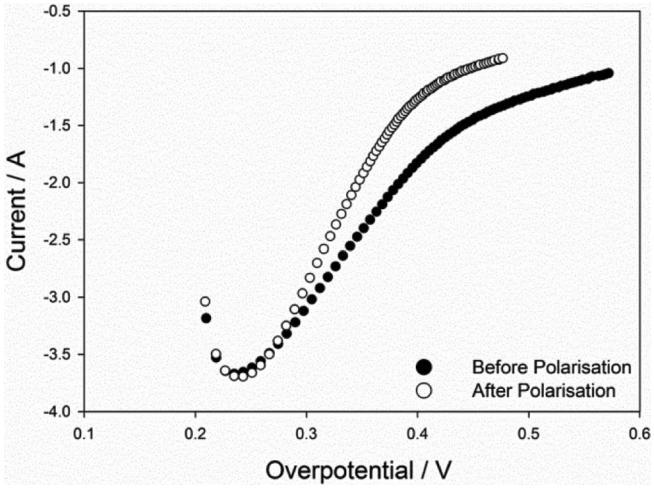

Figure 6. Tafel plot comparison for a 25 mol% Ni 75 mol% Ru electrode before and after polarizing at 300 mA cm^{-2} for 10 hours. Electrolyte is 1 M NaOH. Scan rate: 1 mV s^{-1}.

polarized in basic media, the formation of $Ni(OH)_2$/NiOOH occurs from the as deposited crystalline NiO. This gives further support to our earlier assumption which likens our thermal NiO to the multicycled hydrous nickel oxide discussed previously, as this also involves the same $Ni(OH)_2$/NiOOH redox couple. The mixed oxide electrodes display a different behavior upon multicycling/polarization in contrast to either RuO_2 or NiO. Taking a 25 mol% RuO_2 electrode for example, outlined in Fig. 6, the measured Tafel slope and OER current densities were found to be invariant upon successive steady state polarization measurements, in contrast to the response observed for the two individual oxides. Both discrete oxides were found to vary either in Tafel slope or current density when subjected to these successive potential sweeps. This would lead one to believe that any simple linear superposition response of the two oxides is not occurring here. More interestingly, upon subjecting this film to a fixed current density of 300 mA cm^{-2} for 10 hours, the Tafel slope was found to decrease from ca. 75 mV dec^{-1} to ca. 50 mV dec^{-1}, and the OER current density was found to increase by a factor of three over that of the 'fresh' electrode at a fixed overpotential of 0.4 V as shown in Fig. 6. It is clear therefore that we are seeing 'the best of both worlds' type behavior when using this oxide mixture. We observe the lowering of the Tafel slope upon polarization, indicative of NiO, and concurrently note an increase in the OER current density which indicative of RuO_2, when subjected to a prolonged large current density. This enhancement in performance is in direct contrast to what is observed for a 75 mol% RuO_2 electrode where negligible change in Tafel slope or current density was observed when the same polarization regime was applied. From examining the SEM images in Fig. 7 we can see the effect of such polarization has on the 25 mol% RuO_2 electrode. It is clear that upon polarization the presence of an increased amount of RuO_2 surface microparticles occurs which would account for the increase in catalytic activity for the OER. This could be due to preferential dissolution of NiO over RuO_2 but our lifetime study tests shown later does not support this proposal as NiO is found to be extremely stable under such intensive polarization regimes. There is clearly another process occurring here, possibly a migration of RuO_2 to the surface. This is currently under investigation and will be reported in a future publication.

To truly measure how active a catalyst is for the OER many papers often quote key performance indicators (KPI's), such as the OER onset potential, overpotential at a fixed current density, turnover frequency (TOF), and, often omitted; the stability of the catalyst. The OER onset potential is an indicator of how effective the catalyst is at lowering the activation barrier for oxygen evolution. As seen in Fig. 8a, NiO begins to evolve oxygen at overpotential of ca. 0.38 V, in good agreement[28] with values of nickel oxides prepared in the literature using this thermal decomposition method. Significantly, the addition of just 10 mol% RuO_2 to a NiO electrode causes a reduction in OER onset potential of 20%, while the addition of 25 mol% RuO_2 led to a 33% drop in the OER onset potential. We suggest that this significant observed drop in OER onset overpotential is due to surface enrichment by RuO_2 upon oxide mixing, and is excellent agreement with the observed SEM data shown in Fig. 1. With increasing additions however there were diminishing returns in the reduction of the OER onset potential with additions over 25 mol% of RuO_2 having relatively little effect. Juodkazis and co-workers[28] have shown previously for an equimolar mixture of RuO_2 and NiO there was some observed synergistic effects for the OER in alkaline conditions, however only one mole fraction was studied. In addition the authors used a nickel rather than a titanium substrate, which could affect the measured catalytic behavior due to underlying nickel substrate being an effective OER catalyst itself.

A similar trend is also observed when one examines the overpotential at a fixed current density. To obtain a current density one obviously must know the real surface area of the film in question rather than just the geometrical area. Historically there has been controversy in determining the real or electrochemically active surface area of porous oxide electrodes. While there has been theoretical work done on calculating the surface area of compact flat oxides by deriving a surface area conversion factor using the capacitance, there is still debate over calculating the real surface area of porous electrodes such as the ones examined here. Due to this, we have opted to normalize our current using the voltammetric charge which has been suggested by Trasatti[30,31] to accurately represent the amount of electrochemically active surface available for the OER. One obtains the voltammetric charge, often denoted by q*, by integrating the area under the oxidation or reduction sweep of the voltammogram, here we used the oxidation sweep of the cyclic voltammograms shown in Fig. 2, and normalizing for the scan rate. Here, one must assume that all of the electrode surface available for oxidation or reduction is also available for the OER and it has been shown for relative thin films such as the ones used here, that q* is indeed proportional to the measured BET surface area. We do however recognize that the BET surface area will not be exactly the same as the electrochemically active surface area in solution since BET measurements usually utilize an inert gas while in solution we are concerned with hydroxide ion interaction with the surface. Shown in Fig. 8b, there is a marked drop in overpotential for both the high

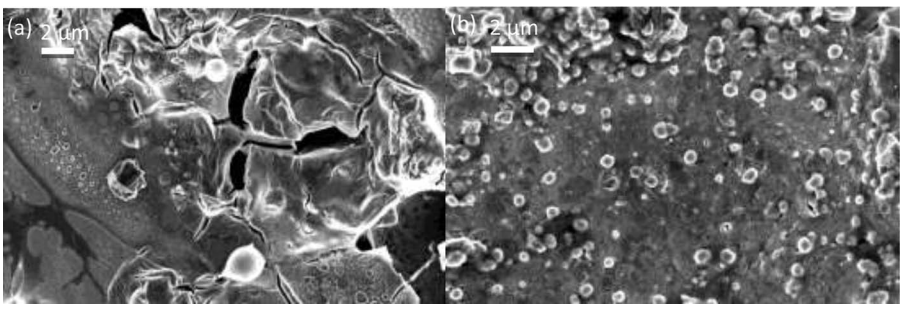

Figure 7. SEM comparison of a 25% Ru 75% Ni electrode (a) before and (b) after polarization at 300 mA cm^{-2} for 10 hours.

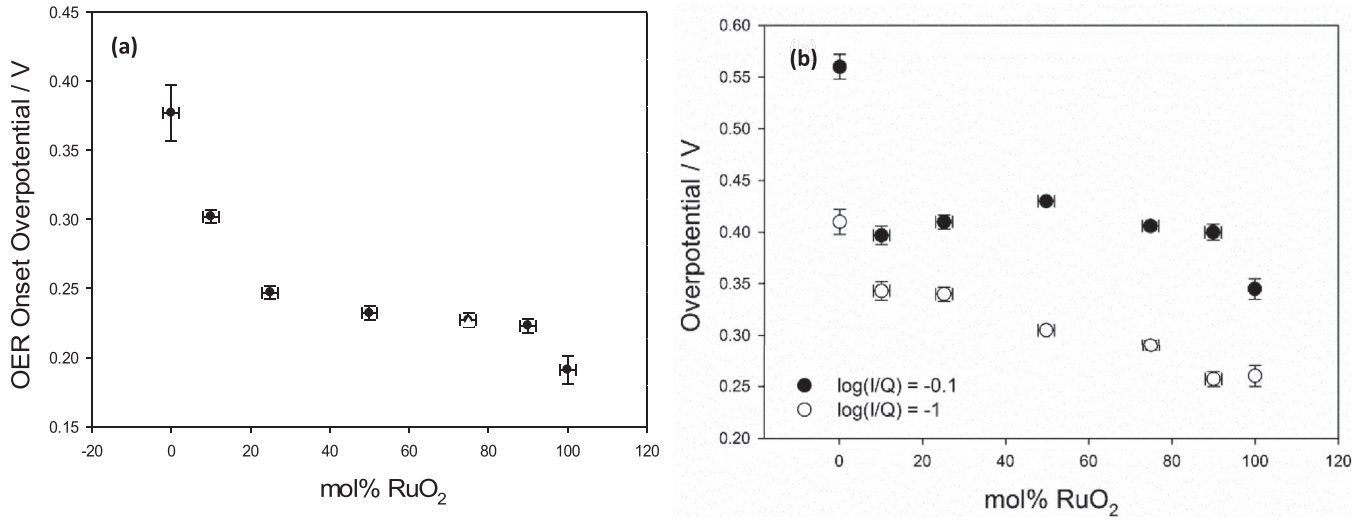

Figure 8. Oxygen evolution reaction onset overpotential as a function of oxide composition. (b) Observed overpotential for oxygen evolution at two fixed currents normalized by voltammetric charge. Electrolyte: 1 M NaOH.

and low current densities chosen, with reductions of 29% and 17% respectively with the addition of 10 mol% RuO_2. The same diminishing returns effect can also be seen here with increasing the relative mol% of RuO_2.

Another useful measure of how catalytic material is in quantifying the TOF. The TOF is often used in heterogeneous catalysis to measure how catalytic a given material is for the reaction in question. The electrochemical TOF can be calculated using a method used by Bell and Yeo[10] and is given by the following expression

$$TOF = \frac{J}{4Q} \quad [7]$$

where J is the current density and Q is the charge density. Q is calculated as per q* mentioned previously. One can easily rationalize this expression by considering the current density as a rate and, as explained previously, relating the charge density to the amount of electrochemically active material in the oxide film so ones ends up with a rate per unit material which is the classical definition of TOF. The factor of four arises from the OER being a four electron transfer process. Fig. 9a shows the increasing exponential like behavior of the OER TOF at a fixed overpotential of 0.2 V with successive increases of RuO_2. This potential was chosen so that all TOFs for all the mixed oxides lie in the same Tafel region which gives one a like for like comparison. With additions up to 75 mol% RuO_2, there is little increase in TOF, suggesting that there is no favorable interaction between the two oxides in contrast to what was observed for the OER onset potential as shown earlier with Fig. 9a suggesting that NiO is hindering the intrinsic activity of RuO_2, which explains the large increase in TOF observed for the pure RuO_2 electrode over that of a 75 mol% RuO_2 film.

Fig. 9b shows accelerated corrosion tests carried out on a sample of mixed oxide compositions. These corrosion tests consisted of polarizing the electrode at 300 mA cm^{-2} for 10 hours in 1 M NaOH. We note that for both RuO_2 and NiO there is very little increase in potential under prolonged polarization. RuO_2 experiences a slight increase initially in potential, most likely due to the spalling of oxide material which is loosely bound to bulk oxide film. NiO on the other hand experiences a drop in potential over the first 5000 s of polarisarion indicating an increase in catalytic activity. This is possibly due to the creation of anodically formed catalytic NiOOH from the as deposited NiO. Trotochaud and co-workers have shown such growth when thin NiO films were subjected to current densities as low as 10 mA cm^{-2} for six hours.[29] We see that for both oxide mixtures shown here that there is a slight increase in the cell potential when subjected to the

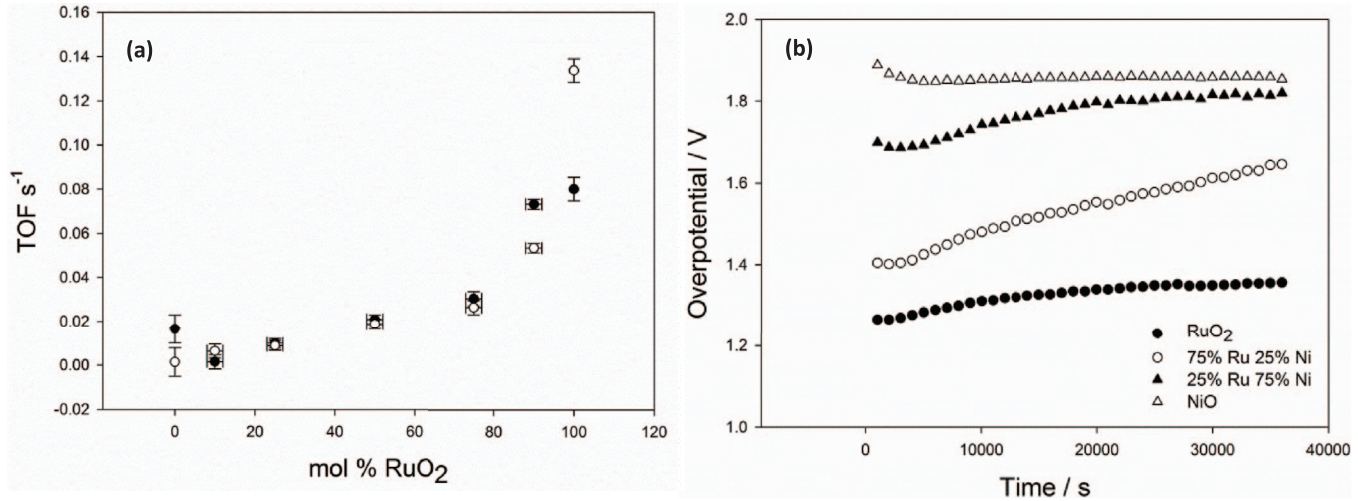

Figure 9. (a) Turnover frequency values as a function of oxide composition both as prepared and 'used'. (b) Lifetime tests for two mixed oxides. Films polarized at 300 mA cm^{-2} for 10 hours. Electrolyte: 1 M NaOH.

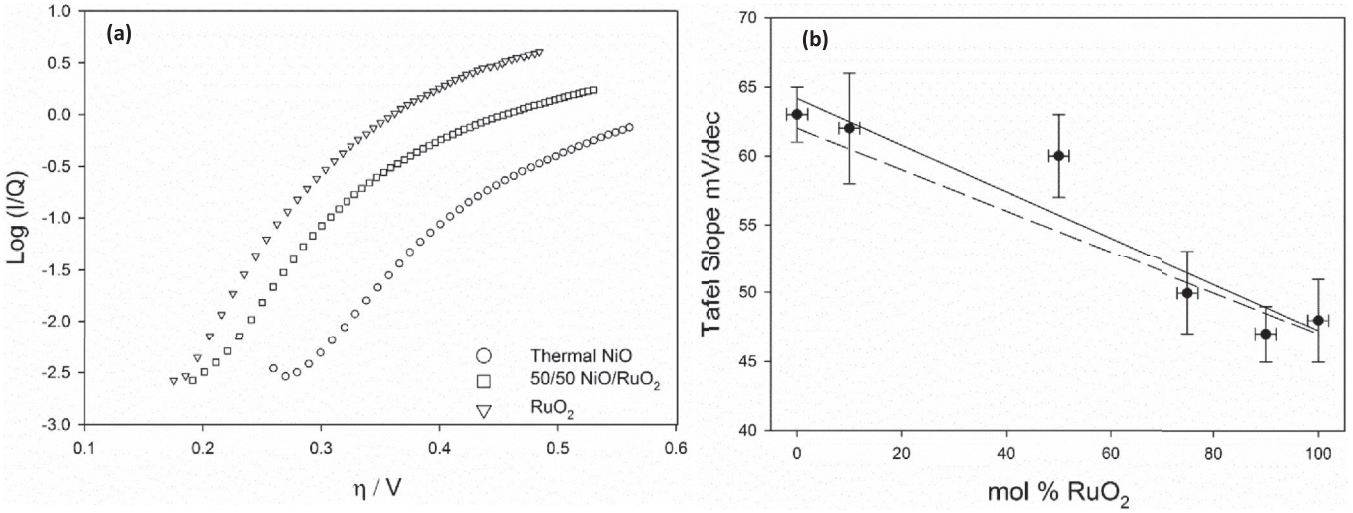

Figure 10. (a) Tafel slope as a function of mol% RuO_2 for a mixed NiO/RuO_2 system. Predicted line (dashed) if the Tafel slope was a simple linear superposition of the two discrete oxides (b) Sample Tafel plots of mixed oxide compositions studied.

corrosion regime. The electrode containing a majority of NiO, although displaying a larger overpotential, is markedly more stable under prolonged polarization with little or no increase in potential observed >20 000 s while the predominantly RuO_2 electrode experiences, albeit a slower increase after >10 000 s, increase in overpotential for the duration of the lifetime test.

Kinetic analysis of the OER.— To elucidate a possible reaction mechanism for the OER it is pertinent to examine the relevant kinetics involved. Two experimental kinetic parameters often examined in analysis of the OER are the Tafel slope, b, and reaction order m_{OH^-}, with respect to hydroxide ion which is given by the following expression:

$$m_{OH^-} = \frac{\partial \log I}{\partial \log a_{OH^-}} \quad [8]$$

where I is the current and a_{OH^-} is the activity of the hydroxide ion. Experimentally we calculate m_{OH^-} by plotting several Tafel scans in differing base concentrations, typically in the range of 0.5–5 M and measuring the current at a fixed overpotential in each concentration. We equate the current with the rate of reaction and thus the classical rate equation holds. Herein a Hg/HgO reference electrode is used. If the composition of the reference electrode is kept constant (say 1.0 M NaOH) and the base concentration of the working electrode compartment varied during reaction order measurements, then the reaction order measured is $m_{OH^-,E}$ where E is the potential. In contrast, if the solution in the reference electrode compartment is the same as that under investigation, the pertinent reaction order is $m_{OH^-,\eta}$. Therefore we measured the reaction order at constant potential which gives the kinetically and chemically significant reaction order. The relationship between the two can be given by $m_{OH^-,\eta} = m_{OH^-,E} - \beta$ where β is the symmetry factor. The Tafel slope can give mechanistic insight into the relevant rate determining step (RDS) in a multistep electron transfer process and is intrinsically also a measure of catalytic activity. Fig. 10a shows Tafel plots in 1 M NaOH for a sample of the oxide compositions studied. The Tafel slope was found to vary in a near linear fashion from ca. 63 mV/dec for a NiO electrode to ca. 48 mV/dec for a RuO_2 electrode as can be depicted in Fig. 10b. Our experimental value of 62 ± 2 mV for the Tafel slope and reaction order of 0.86 ± 0.06 (Fig. 11a) obtained for NiO agrees excellently with the kinetic parameters obtained for hydrous nickel oxides/hydroxides prepared by potential multicycling and electroprecipitation.[21,33] Interestingly, we observe a fractional reaction order (Fig. 11b) of approx. 0.5 for RuO_2 and all other mixed oxide materials studied. The observed value of a fractional reaction order differs from that previously reported by Lyons and Floquet[4] and others[32] observed a reaction order of unity

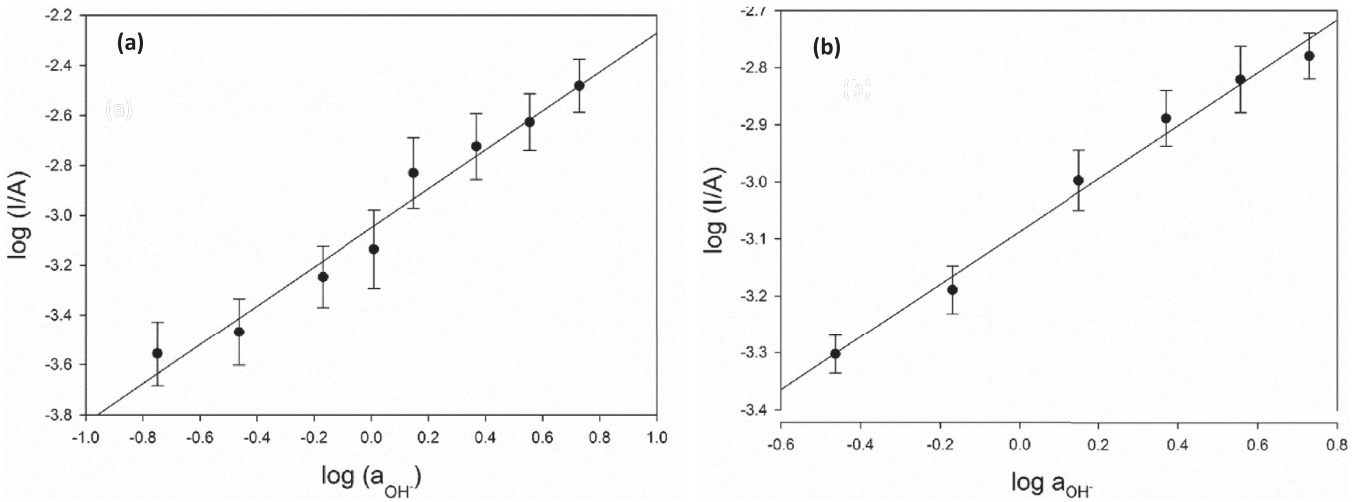

Figure 11. (a) Reaction order plot of (a) NiO at η = 0.352 V. Slope: 0.86 and (b) RuO_2 at η = 0.222 V. Slope: 0.49.

for RuO_2. We propose a dual barrier model (DBM) further on to account for this difference in observed reaction order for RuO_2. Using the kinetic data obtained, we propose a possible OER mechanism at NiO and RuO_2 surfaces. We have previously reported a proposed mechanism for the OER at metal oxides based on the surfaquo group concept which has the advantage of enabling a direct relationship to molecular water catalysis.[20] We will initially detail our proposed general mechanism for the OER at these metal oxide surfaces, which predicts our kinetic data for NiO, and subsequently use a modification employing a dual barrier model to account for the fractional reaction order obtained for RuO_2 and indeed all mixed oxide compositions containing RuO_2. The proposed catalytic cycle for the OER is shown below. Step A.I is considered a pre-equilibrium step. The complete reaction can therefore be written schematically as follows:

$$SOH_2 + OH^- \leftrightarrows SOH^- + H_2O \quad \text{(A.I)}$$

$$SOH^- \rightarrow SOH + e^- \quad \text{(A.II)}$$

$$SOH + OH^- \rightarrow SO^- + H_2O \quad \text{(A.III)}$$

$$SO^- \rightarrow SO + e^- \quad \text{(A.IV)}$$

$$SO + OH^- \rightarrow SOOH + e^- \quad \text{(A.V)}$$

$$SOOH + OH^- \rightarrow SO_2 + H_2O + e^- \quad \text{(A.VI)}$$

$$SO_2 + OH^- \rightarrow SOH^- + O_2 \quad \text{(A.VII)}$$

where S represents a surfaquo group attached to the bulk oxide. The surfaquo group concept proposed envisages hydrated interlinked oxy-metal surface active groups, hence the term surfaquo group, which facilitate the OER at the surface. Again, we are likening the OER behavior of NiO prepared by this thermal decomposition method to other nickel oxides/hydroxides formed by potential multicycling in base, electroprecipitation.[33] The nickel cations at the surface tend to undergo some degree of hydration i.e. become coordinated to surrounding water molecules, in the basic environment. The coordinated water molecules are therefore the source of the discharged hydroxide ion in step I. This hydration of thermally prepared NiO is therefore not unreasonable to expect in the strongly alkaline environment used. It is likely that a significant proportion of these coordinated water molecules will be deprotonated due to the pKa value for a water molecule coordinated to a highly charged metal atom being generally in the range between 5–9. On this basis we make the assumption in our reaction scheme that step (I) is facile. The surfaquo group concept attempts to bridge the link between these heterogeneous electrocatalysts and homogeneous molecular catalysts for water oxidation which is an area of current intense study by groups such as Llobet and co-workers.[34,35] The OER catalytic cycle can be seen pictorially in Fig. 12a which shows the octahedrally coordinated surfaquo group attached to the bulk NiO.

We can now conduct a kinetic analysis of the mechanism shown in the scheme above. We envisage the rate determining step for NiO being the formation of the metal oxide SO^- (step II) and the metal-oxo SO (step IV) species due to the high energy associated with the formation of these species. Our rationale is supported by DFT studies carried out by Muckerman and co-workers[36] who showed, that for a GaN/ZnO surface with high coverage of adsorbed OH^- ions the intermediate associated with the highest energy was an oxide radical. Therein, Muckerman and co-workers consider the influence of the solution hydrogen bonding network on the energy of the intermediates and suggest that a metal oxide in contact with solution is energetically more favorable to be ionized rather than be neutral and hence the acid/base behavior of the surfaquo group will be integral to any consideration of the OER. Similarly, Rossmeisl and co-workers[37] performed a DFT study of the OER at RuO_2 surfaces. They too found, for a surface saturated with adsorbed OH, that the highest energy intermediate was a surface oxygen species, in this case an oxo species.

If we assume step (II) is rate determining then the net reaction flux is given by:

$$f_\Sigma = \frac{I}{nFA} = k_2 a_{OH^-} \Gamma_{SOH} \quad [9]$$

where n = no of moles of electrons, F = Faraday's constant, k_2 is the reaction rate constant, a_{OH^-} is the activity of the hydroxide ion and Γ is the surface coverage. Note, our assumption is that there is Langmuir style adsorption which assumes full surface coverage, future work will take into account situations where partial surface coverage i.e. Tempkin adsorption might occur.

$$\Gamma_{SOH} \cong \frac{k_1' \Gamma_{SOH^-}}{k_{-1}' + k_2 a_{OH^-}} \quad [10]$$

Hence, the net reaction flux is given by:

$$f_\Sigma = \frac{k_2 k_1' \Gamma_{SOH^-} a_{OH^-}}{k_{-1}' + k_2 a_{OH^-}} \quad [11]$$

However since k_1' and k_{-1}' are electrochemical rate constants they are therefore potential dependent in contrast to chemical rate constants. We can take this potential dependence into account by utilizing the Butler-Volmer rate equation given by:

$$k_n' = k_n^0 \exp[\beta F\eta/RT] \text{ and } k_{-n}' = k_{-n}^0 \exp[-(1-\beta)F\eta/RT] \quad [12]$$

where η denotes the overpotential, β is the symmetry factor and k_n^0 is the standard chemical rate constant. Hence the net flux, taking into account the potential dependence of k_1' and k_2', can be written as:

$$f_\Sigma = \frac{k_2^0 a_{OH^-} \Gamma_{SOH^-} k_1^0 \exp[\beta F\eta/RT]}{k_{-1}^0 \exp[-(1-\beta)F\eta/RT] + k_2 a_{OH^-}} \quad [13]$$

Now, if step (II) is rate determining then we can say with assurance that $k_2^0 \ll k_{-1}^0$ and therefore eqn 13 simplifies to give:

$$f_\Sigma = k_2^0 \Gamma_{SOH^-} a_{OH^-} \frac{k_1^0}{k_{-1}^0} \exp[\beta F\eta/RT] \quad [14]$$

This expression therefore predicts a reaction order of 1 with respect to OH^- activity and a Tafel slope of ca. 60 mV dec^{-1} at 298 K assuming $\beta = \frac{1}{2}$ which is reasonable since this value assumes that any intermediate species generated have an energy profile halfway between the starting species and the product. The theory thus agrees well with our experimental results for NiO. The kinetic data obtained for an RuO_2 electrode can also be incorporated into a proposed mechanism for the OER. The following mechanism was previously proposed by Lyons and Floquet[11] and has been adapted for use here and, similarly to scheme A, starts with the initial discharge of a hydroxide ion. A more in depth analysis of the mechanism can be found in an extensive review of the OER at metal oxides published recently by our group.[17] This hydroxide discharge is then thought to be followed by a structural rearrangement to a more energetically favorable arrangement to accommodate the extra hydroxide ion. Subsequent to this rearrangement, a second electron discharge occurs forming an unstable Ru (VIII) species which acts as a precursor to the generation of oxygen. The relevant OER mechanistic steps, which incorporate the surfaquo group concept for RuO_2 are given by the following scheme:

$$(-O-)_2 RuO^-(OH)_3 + OH^- \leftrightarrow (-O-)_2 Ru.O^-(OH)_2 + H_2O + e^- \quad \text{(B.I)}$$

$$(-O-)_2 RuO.O^-(OH)_2 \rightarrow (-O-)_2 RuO_2(OH)_2 + e^- \quad \text{(B.II)}$$

$$(-O-)_2 RuO_2(OH)_2 + 2OH^- \rightarrow (-O-)_2 RuO_2 + 2H_2O + O_2 + 2e^- \quad \text{(B.III)}$$

$$(-O-)_2 RuO_2 + OH^- + H_2O \rightarrow (-O-)_2 RuO^-(OH)_3 \quad \text{(B.IV)}$$

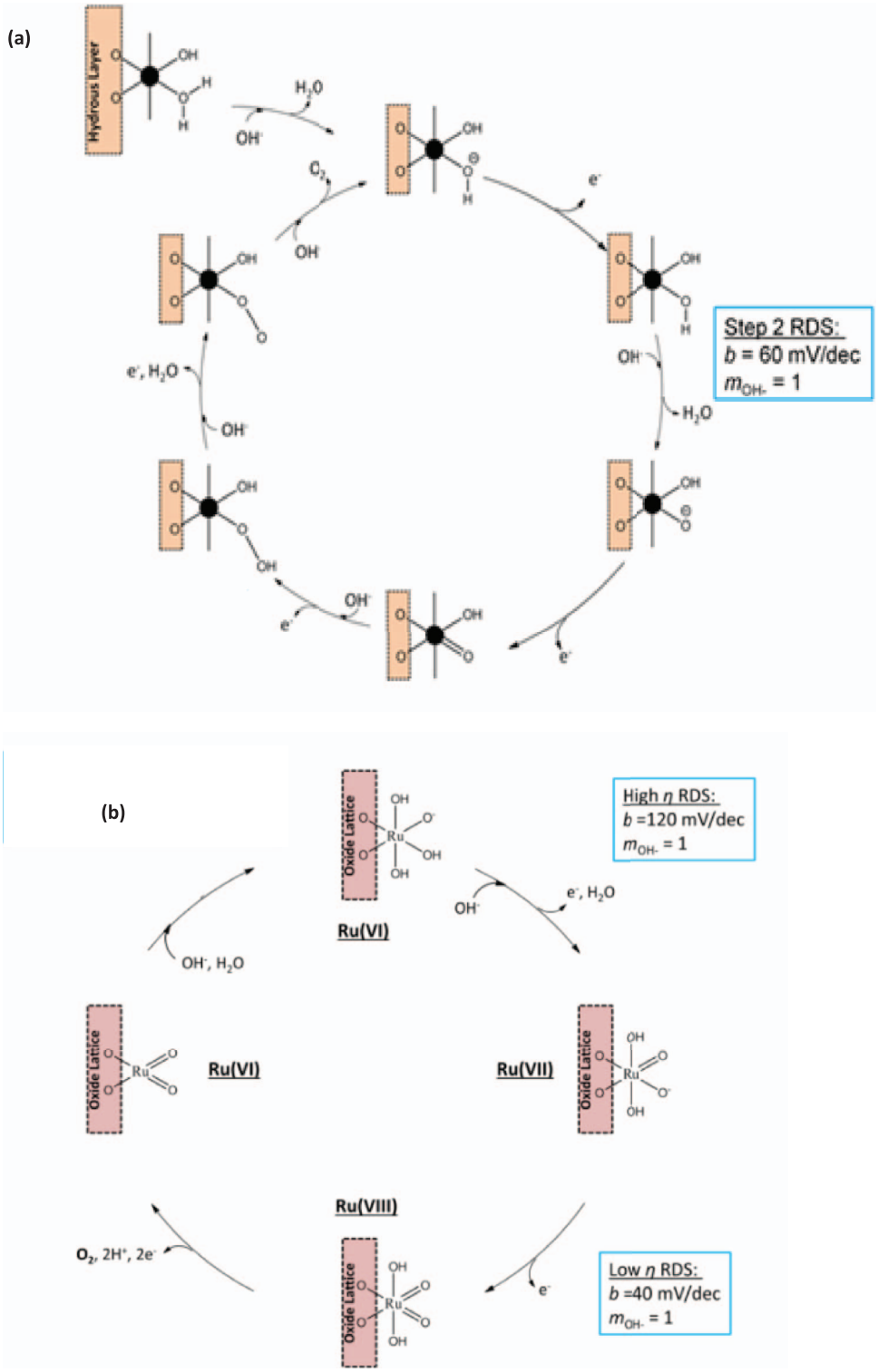

Figure 12. Pictorial representation of the oxygen evolution reaction for (a) NiO (b) RuO_2 in base involving catalytically active surfaquo groups bound to the outer hydrous layer by bridging oxygens. This model assumes complete surface coverage. RDS: Rate determining step, b: Tafel slope, m_{OH^-} : Reaction order.

Scheme B is represented pictorially in Fig. 12b, and Lyons and Floquet arrive at a theoretical expression for the total flux given by:

$$f_\Sigma = \frac{k_1^0 k_2^0 \Gamma_S a_{OH} - \exp[\beta\eta]}{k_{-1}^0 a_{H2O} \exp[-\eta] + k_2^0} \qquad [15]$$

and at low overpotentials assuming $k_2^0 \ll k_{-1}^0$ eqn 15 reduces to:

$$f_\Sigma = K^0 a_{H2O}^{-1} \Gamma_s a_{OH^-} \exp[(1+\beta)\,\eta] \qquad [16]$$

which predicts a reaction order of unity and a Tafel slope of 40 mV dec^{-1}. Interestingly, and in contrast to Lyons and Floquet, we have obtained an experimental reaction order value of 0.48 ± 0.05 We

propose a dual barrier model developed by MacDonald and Conway[37] to rationalize the difference in our experimental Tafel slope and reaction order to that shown in the literature as mentioned previously. This model, owing much to earlier work by Meyer,[38] envisages that only a fraction of the total potential difference between the metallic electrode and the electrolyte is effective in lowering the potential barrier to interfacial electron transfer. In series with this, the remainder of the potential drop occurs across an electronically conducting 'barrier' oxide, through which the charge passed in the OER must migrate under the influence of an electric field. The barrier here we are considering is the barrier at the inner compact oxide/thin outer hydrated oxide interface like the one proposed by Burke and O'Sullivan which is discussed more detail in a previous review of such oxides.[17] They suggest the significant potential drop in such oxides is across this interface with minimal potential drop occurring through the inner compact oxide which is largely conducting. It is worth noting here that there is some disagreement over the nature of this potential drop. In the case of gold electrodes, Lohrengel and Schultze[39] observed that the main potential drop is in the compact gold oxide whereas hydrous gold oxide is a good ionic and electronic conductor. Also, in the original paper by Conway, where the dual barrier model is proposed, the compact oxide is suggested to be the main barrier for electrons. Similarly, a number of authors have pointed to a poorly conducting compact platinum oxide in the explanation of OER on Pt oxide/Pt interface.[40] In terms of the Burke O'Sullivan model, if the outer hydrated layer is thin a linear potential drop across the latter may be proposed. If the hydrated layer is thick, then the potential drop extends further into the hydrous layer as illustrated in Fig. 13.[17] While RuO_2 and NiO may have different

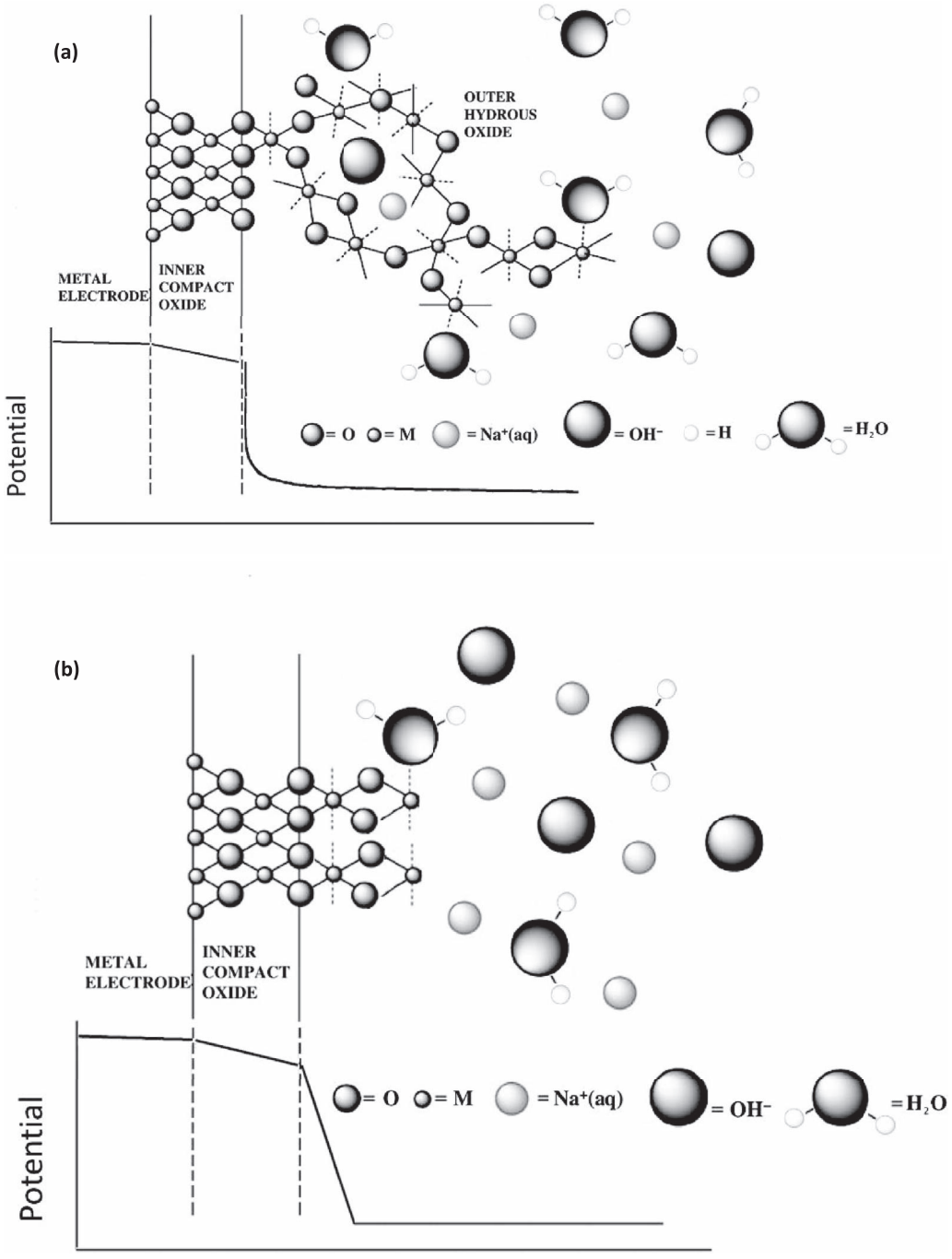

Figure 13. (a) Pictorial representation of potential drop across thick hydrous oxide film. (b) thin hydrous oxide film.

bulk conductivities, what we are concerned with here is the potential drop at the bulk compact oxide/thin outer hydrated oxide interface rather than the potential drop through the bulk oxide. We propose that both oxides contain such a thin hydrated outer oxide layer which is catalytically active. We can justify the use of the DBM here for both oxides by looking at their high frequency impedance response. At high frequencies one expects only to see combined solution and film resistance. As shown in Fig. 3 earlier, we can see that the high frequency impedance response is very similar for RuO_2 and NiO. Since we are using a fixed cell geometry and electrolyte for each oxide film we can assume the solution resistance is constant and therefore the apparent film resistance (using this this preparation procedure) for both oxides is approximately the same. Thus we propose the applicability of the DBM is equally valid for both RuO_2 and NiO. The similarity in high frequency impedance response gives further creed to our assumption that the biggest barrier to electron transfer is at the compact/hydrous oxide interface since RuO_2 has a larger bulk conductivity over NiO but yet give a similar response due to similar hydrous/compact oxide interfaces being present in both. However as we have obtained a reaction order value of close to unity for NiO this barrier is evidently less marked for NiO than RuO_2 and we are currently unaware why this is the case.

Under a normal kinetic analysis of step B.II, the overall rate equation takes the general form:[8]

$$i = i_o \exp\left(\frac{(1+\beta_s)\,\mathrm{F}\eta}{\mathrm{RT}}\right) \qquad [17]$$

where i_o is the exchange current density for the OER and β_s denotes the symmetry factor for the interfacial electron transfer process. If the OER is proceeding in the steady state under dual barrier conditions, the RDS must be in equilibrium with the barrier film charge migration process. Therefore it is possible to obtain an expression for the overall current density across the two barriers by equating eqn. 17 with the rate equation for the oxide charge migration. It can be shown that the resulting expression has the form:[38,39]

$$i = A a_{OH^-}{}^{m_{eff}} \exp\left(\frac{(1+\beta_\Sigma)\,F\eta}{RT}\right) \qquad [18]$$

where m_{eff} is the effective reaction order and β_Σ is the composite symmetry factor given by:

$$\beta_\Sigma = \frac{\beta_F \beta_S}{\beta_F + \beta_S} \qquad [19]$$

where β_F is the symmetry factor for field assisted charge transport through the oxide and β_S represents the symmetry factor for the rate determining interfacial electron transfer reaction, and A denotes the pre-factor. Note that the effective reaction order with respect to hydroxide ion activity is:

$$m_{eff} = \frac{\partial \log i}{\partial \log a_{OH^-}} = \frac{m_{OH^-}\beta_F}{\beta_F + \beta_S} \qquad [20]$$

where m_{OH^-} is the expected value of the reaction order, a value of unity for RuO_2, under more usual single interfacial electron transfer barrier conditions. Thus, if both potential barriers are assumed to be symmetrical $\beta_F = \beta_S = \frac{1}{2}$, and thus $\frac{\partial logi}{\partial log a_{OH^-}}$ will give a reaction order value of 0.5 which agrees excellently with the value 0.48 ± 3 obtained.

As stated before, all oxide compositions containing RuO_2 studied gave a reaction order of ca. 0.5 indicating that RuO_2 dominates the behavior in this regard. One suggestion to account for this observation could be due to the surface enrichment by RuO_2 on the mixed oxide system. Thus if RuO_2 experiences this large potential drop across the compact oxide/thin hydrous oxide interface as described by the DBM then it is possible that due to surface enrichment in the mixed oxide system that this potential drop is also present for all oxide mixtures containing RuO_2. However further work is needed to verify this. As the PXRD data suggests that the mixed oxide system contains two discrete phases rather than forming a new phase, we envisage that the OER mechanism of the mixed oxides will simply be a combination of the two discrete mechanisms rather than a new mechanism being involved. Indeed the linear superposition type behavior of the Tafel slopes supports this theory.

Conclusions

In conclusion, we have developed a simple preparation method for RuO_2/NiO mixed oxide catalysts prepared by thermal decomposition. RuO_2 and NiO were both shown to activate when subjected to repeated polarization regimes with a decrease in Tafel slope and increase in OER current density respectively. Addition of just 10 mol% RuO_2 to a NiO electrode was found to decrease the OER onset potential by 20% with increasing additions having significantly diminishing returns. The OER current densities for the 25/75 mol% RuO_2/NiO electrode was found to significantly increase when preconditioned to prolonged polarization regimes with the Tafel slope also decreasing from ca. 75 mV dec^{-1} to ca. 50 mV dec^{-1}. NiO prepared in this manner was found to be electrochemically similar to other nickel oxides prepared using different methodologies and we have proposed a similar OER mechanism based on the kinetic data obtained using the surfaquo group concept. A near unity value for the reaction order was seen for NiO which is in accordance with values obtained for nickel oxides/hydroxides prepared using different methodologies. A dual barrier model was used to rationalize the fractional reaction order of ca. 0.5 obtained for RuO_2. Due to the surface enrichment of RuO_2 exhibited by the RuO_2/NiO mixed oxide films over a large range of compositions, it is therefore not unexpected that a fractional reaction order was observed.

Acknowledgments

This publication has emanated from research conducted with the financial support of Science Foundation Ireland under grant number SFI/10/IN.1/I2969 and SFI/12/RC/2278.

References

1. S. Trasatti, *Electrochimica Acta*, **45**, 2377 (2000).
2. Z. S. Msindo, V. Sibanda, and J. H. Potgieter, *J. Appl. Electrochem.*, **40**, 691 (2010).
3. M. E. G. Lyons and L. D. Burke, *J. Chem. Soc., Farad. Trans. 1: Physical Chemistry in Condensed Phases*, **83**, 299 (1987).
4. S. Floquet and M. E. G Lyons, *Phys. Chem. Chem. Phys.*, **13**, 5314 (2011).
5. F. Tantardini, S. Trasatti, and D. Galizzioli, *J. App. Electrochem.*, **4**, 47 (1974).
6. F. Tantardini, D. Gallizioli, and S. Trasatti, *J. App. Electrochem.*, **5**, 203 (1975).
7. E. Sivieri, G. Lodi, A. De Battisti, and S. Trasatti, *J. App. Electrochem.*, **8**, 135 (1978).
8. M. E. G. Lyons and M. P. Brandon, *J. Electroanal. Chem.*, **641**, 119 (2010).
9. L. Russell, M. E. G. Lyons, M. O'Brien, R. L. Doyle, I. Godwin, and M. P Brandon, *Int. J. Electrochem. Sci.*, **7**, 2710 (2012).
10. B. S. Yeo and A. T. Bell, *J. Phys. Chem. C*, **116**, 8394 (2012).
11. W. M. Keely and H. W. Maynor, *J. Chem. Eng. Data*, **8**, 297 (1963).
12. M. A. A. Elmasry, A. Gaber, and E. M. H. Khater, *J. Therm. Anal. Calorim.*, **52**, 489 (1998).
13. G. Singh, M. H Miles, and S. Srinivasan, Electrocatalysis on Non-Metallic Surfaces, Proceedings of Workshop held at NBS, Gaithersburg, Dec 9-12, 1975.
14. L. M. Da Silva, J. F. C. Boodts, and L. A. DeFaria, *Electrochim. Acta*, **45**, 2719 (2000).
15. N. Krstajic and S. Trasatti, *J. Appl. Electrochem.*, **28**, 1291 (1998).
16. G. Novell-Leruth, G. Carchini, and N. Lopez, *J. Chem. Phys.*, **138**, 194706 (2013).
17. L. D. Burke and E. J. M. O'Sullivan, *l. Electroanal. Chem.*, **117**, 155 (1981).
18. J. McBreen, in *Handbook of Battery Materials*, . J. O. Besenhard, Wiley-VCH, Weinheim, 2007.
19. P. W. T. Lu and S. Srinivasan, *J. Electrochem. Soc.*, **125**, 1416 (1978).
20. R. L. Doyle, I. J. Godwin, M. P. Brandon, and M. E. G. Lyons, *Phys. Chem. Chem. Phys.*, **15**, 13737 (2013).
21. I. J. Godwin and M. E. G. Lyons, *Electrochem. Comm.*, **32**, 39 (2013).
22. M. E. G. Lyons, R. L. Doyle, and M. P. Brandon, *Phys. Chem. Chem. Phys.*, **13**, 21530 (2011).
23. L. D. Burke, M. E. Lyons, and O. J. Murphy, *J. Electroanal. Chem.*, **132**, 247 (1982).
24. E. J. M. O'Sullivan and L. D. Burke, *J. Electrochem. Soc.*, **137**, 466 (1990).
25. L. D. Burke and R. A Scannell, *Platinum Met. Rev.* **28**, 56 (1984).
26. M. E. G. Lyons and L. D. Burke, *Modern Aspect of Electrochemistry*, **18**, 169 (1986).
27. J. A. M Simões and J. L Beauchamp, *Chem. Rev.*, **90**, 629 (1990).
28. K. Juodkazis, J. Juodkazytė, R. Vilkauskaite, B. Sebeka, and V. Jasulaitiene, *Chemija*, **19**, 1 (2008).
29. L. Trotochaud, J. K. Ranney, K. N. Williams, and S. W. Boettcher, *J. Am. Chem. Soc.*, **134**, 17253 (2012).

30. S. Trasatti. *Electrochim. Acta*, **36**, 225 (1991).
31. S. Trasatti, J. Lipkowski, and P. N. Ross, *The Electrochemistry of Novel Materials*, vCH Publishers Inc., 1994.
32. Y. Matsumoto and E. Sato, *Mat. Chem. Phys.*, **14**, 397 (1986).
33. A. Cakara, I. Godwin, R. L. Doyle, P. O'Brien, and M. E. G. Lyons, *Int. J. Electrochem. Sci.*, **7**, 11768 (2012).
34. L. Duan, F. Bozoglian, S. Mandal, B. Stewart, T. Privalov, A. Llobet, and L. Sun, *Nat. Chem.*, **4**, 418 (2012).
35. A. Llobet, *Nat Chem.*, **2**, 804 (2010).
36. Shen Y. A. Small, J. Wang, P. B. Allen, M. V. Fernandez-Serra, M. S. Hybertsen, and J. T. Muckerman, *J. Phys. Chem. C*, **114**, 13695 (2010).
37. J. J. McDonald and B. E. Conway, *Proc. R. Soc. London, Ser. A*, **269**, 419 (1962).
38. R. E. Meyer, *J. Electrochem. Soc.*, **107**, 847 (1960).
39. M. M. Lohrengel and J. W. Schultze, *Electrochim. Acta*, **21**, 957 (1976).
40. A. Damjanovic and B. Jovanovic *J. Electrochem. Soc.* **123**, 374 (1976).